$La_{0.8}Sr_{0.2}Ga_{0.83}Mg_{0.17}O_{3-\delta}$ PEROVKITES INVESTIGATED BY IMPEDANCE SPECTROSCOPY AND X-RAY PHOTOELECTRON SPECTROSCOPY

Rareş SCURTU[1], Gheorghe NECHIFOR[2], Cristian ANDRONESCU[3], Victor FRUTH[4], Petre OSICEANU[5]

$La_{0.8}Sr_{0.2}Ga_{0.83}Mg_{0.17}O_{3-\delta}$ nanopowders were prepared by sol-gel method and they were calcinated at three different temperatures 900°C, 1000°C and 1200°C. The aim of this article was to investigate the role of precalcination temperatures on the physicochemical properties of the obtained LSGM powders. XPS data confirmed the presence of the dopants in the material and allowed to identify two different chemical states for Sr^{2+} and oxygen both related to the oxygen-deficient perovskite structure of LSGM. The sample calcinated at 1200°C exhibited an electrical conductivity at 627°C (typical operating temperature for IT-SOFCs), with 200% and 500% higher than those calcinated at 1000°C and 900°C, respectively.

Keywords: impedance spectroscopy, XPS, LSGM, IT-SOFC electrolyte

1. Introduction

Solid Oxide Fuel Cells (SOFCs) have attracted worldwide interest for their high energy conversion efficiency (50 % – 70 %), structure integrity, easy operation, less impact to environment and for their high tolerance to fuels [1, 2]. Due to the high operating temperatures (900 °C – 1000 °C), the requirements imposed to the materials that constitute the cells with solid oxide electrolyte, to produce them is very restrictive. In response to these challenges, intermediate temperature solid oxide fuel cells (IT-SOFCs) are being developed to reduce high-temperature material requirements, which will extend useful lifetime, improve durability and reduce cost, while maintaining good fuel flexibility [3, 4]. A major challenge in reducing the operating temperature (600 °C – 800 °C) of SOFCs is

[1] Postdoctoral Researcher, National Institute for Research and Development in Microtechnologies, Bucharest, Romania, e-mail: rares.scurtu@gmail.com
[2] Prof., Department Chemistry Engineering, Faculty of Applied Chemistry and Materials Science, University POLITEHNICA of Bucharest, Romania
[3] PhD Student, Department Oxide Compounds and Materials Science, Institute of Physical Chemistry, Romanian Academy, Bucharest, Romania
[4] Scientific Researcher, Department Oxide Compounds and Materials Science, Institute of Physical Chemistry, Romanian Academy, Bucharest, Romania
[5] Scientific Researcher, Department Surface Chemistry and Catalysis, Institute of Physical Chemistry, Romanian Academy, Bucharest, Romania

the development of solid electrolyte materials with sufficient conductivity to maintain acceptably low ohmic losses during operation.

A promising candidate as electrolyte material for intermediate temperature SOFCs is the perovskite type oxide $LaGaO_3$ doped with Sr and Mg (LSGM) which exhibits a greater conductivity than the conventional stabilized zirconia electrolytes [5]. The perovskites (ABO_3) consist of 12-fold coordinated large cations of A and 6-fold coordinated small cations of B [6-8]. Thus, the $LaGaO_3$ is the base compound in which the La and Ga sites can be doped with divalent ions with the proper size. Sr^{2+} and Mg^{2+} are favorable dopants due to their low solution energies [1]. Oxygen vacancies are formed according to the fallowing equations:

$$2SrO \xrightarrow{LaGaO_3} 2Sr'_{La} + V_O^{\cdot\cdot} \quad (1)$$

$$2MgO \xrightarrow{LaGaO_3} 2Mg'_{Ga} + V_O^{\cdot\cdot} \quad (2)$$

The ionic conductivity increases with amount of Sr dopand which increase the amount of oxygen vacancies, but when Sr content become higher than 10 % mol the solid solubility of Sr into La sites of $LaGaO_3$ is poor and the insulated secondary phases of $SrGaO_3$ or La_4SrO_7 are formed. The ionic conductivity of LSGM is further increased by increasing the amount of doped Mg, which can attain a maximum of 20 mol% Mg doped on Ga sites. Due to the enlarged crystal lattice the solubility of Sr into $LaGaO_3$ increases up to 20 % mol by doping Mg for Ga sites [9]. The highest oxide ion conductivity in $LaGaO_3$-based oxides is obtained at the compositions of $La_{0.8}Sr_{0.2}Ga_{0.85}Mg_{0.15}O_3$ and $La_{0.8}Sr_{0.2}Ga_{0.8}Mg_{0.2}O_3$ [10].

The LSGM has good conductivity but the ohmic losses can be diminishes more by obtaining thinner electrolyte. The sol-gel method can produce LSGM fine powders with high homogeneity which can be used for obtaining thin films. The focus of this article was to investigate by impedance spectroscopy and XPS and the role of precalcination temperature step on the physicochemical proprieties of the LSGM sample obtained by sol-gel method.

The total electrical conductivity values and apparent activation energies were in good agreement with published data on samples with similar composition but prepared by solid-state route. Therefore, the physicochemical and electrical conductivities confirmed the ability of the sol-gel method to produce LSGM perovskites which represent promising solid electrolyte for SOFCs.

2. Experimental

The LSGM powders were synthesized by Pechini [11] method using as precursors the following $La(NO_3)_3 \times 6H_2O$, $Sr(NO_3)_2$, $Mg(NO_3)_2 \times 6H_2O$, $Ga(NO_3)_3 \times XH_2O$, acid citric and alcool polivinilic. To obtain the powders the

formed gel was heated in the mantle oven up to 150 ºC until solid foam was formed. The foam was then ground and split in three samples which they were heated up to 900 ºC, 1000 ºC and 1200 ºC respectively, at 10 ºC / min and held them at this temperature for 6 h. This precalcination step is necessary for decompose all remaining organic residuals and to form Ga-containing phases thus avoiding the formation of Ga_2O_3 that could decompose to Ga_2O and O_2 at high sintering temperatures [12]. The powders were then ground in an agate mortar and then uniaxially pressed at 350 MPa using a 13mm cylindrical die. The pellets were sintered in air at 1450 ºC for 6 h, with a heating rate of 10 ºC / min. The densities of the sintered pellets were determined by Archimede's technique and were larger than 94%.

The structure of the obtained materials was determined by X-ray diffraction (Rigaku ULTIMA IV Diffractometer, CuKα). The search for impurity phases included the following substances: LSGM, $LaSrGaO_4$ (Powder Diffraction File (PDF) No. 24–1208), $SrLaGa_3O_7$ (PDF No. 45-0637), $La4Ga_2O_9$ (PDF No. 37–1433), and $SrGa_2O_4$ (PDF No. 72-0222).

Surface analysis performed by X-ray photoelectron spectroscopy (XPS) was carried out on PHI Quantera equipment with a base pressure in the analysis chamber of 10^{-9} Torr. The X-ray source was monochromatized Al Kα radiation (1486.6 eV) and the overall energy resolution is estimated at 0.70 eV by the full width at half-maximum (FWHM) of the Au 4f7/2 photoelectron line (84 eV). Although the charging effect was minimized by using a dual beam (electrons and Ar ions) as neutralizer, the spectra were calibrated using the C 1s line (BE = 284.8 eV) of the adsorbed hydrocarbon on the sample surface (C–C or $(CH)_n$ bondings). As this spectrum was recorded at the start and the end of each experiment the energy calibration during experiments was quite reliable. The accuracy for Binding Energies (BEs) assignments was ± 0.2 eV while for quantitative analysis was found in the range ± 10%.

The electrical conductivities were measured by ac impedance spectroscopy. The measurements were carried out with a Solartron 1260 FRA using a ProboStat sample holder (NorECs) heated up by Elite TSV12/50/300 furnace. The impedance spectroscopy measurements were conducted in air, in the temperature range of 100 – 827 °C, over the frequency range of 1 Hz – 1 MHz and the amplitude of alternative signal was 100 mV. The temperature was acquired by using a Pt-Rh thermocouple located close to the sample. For a good contact with the electrodes, two Ag electrodes were pasted on samples surfaces and fired at 600 °C for 1 hour. The experimental data were corrected for the stray capacitance of the sample holder and the resistance and inductance of the measuring leads by using Zview2 fitting software[13].

3. Results and discussion

3.1. XRD results

The structures of the sintered pellets at 1450 °C, as determined by XRD measurements, are presented in Fig. 1 in comparison with the XRD patterns of the initial powders thermally treated at 900 °C, 1000 °C and 1200 °C. It can be seen that the perovskite phase was identified in the pattern of the calcined samples, but other intermediate phases, including $SrLaGa_3O_7$, $La_4Ga_2O_9$, and some trace of carbonates, were also detected. From XRD measurements it seems that the secondary phases were not present in the samples sintered at the temperature of 1450 °C for 6 h.

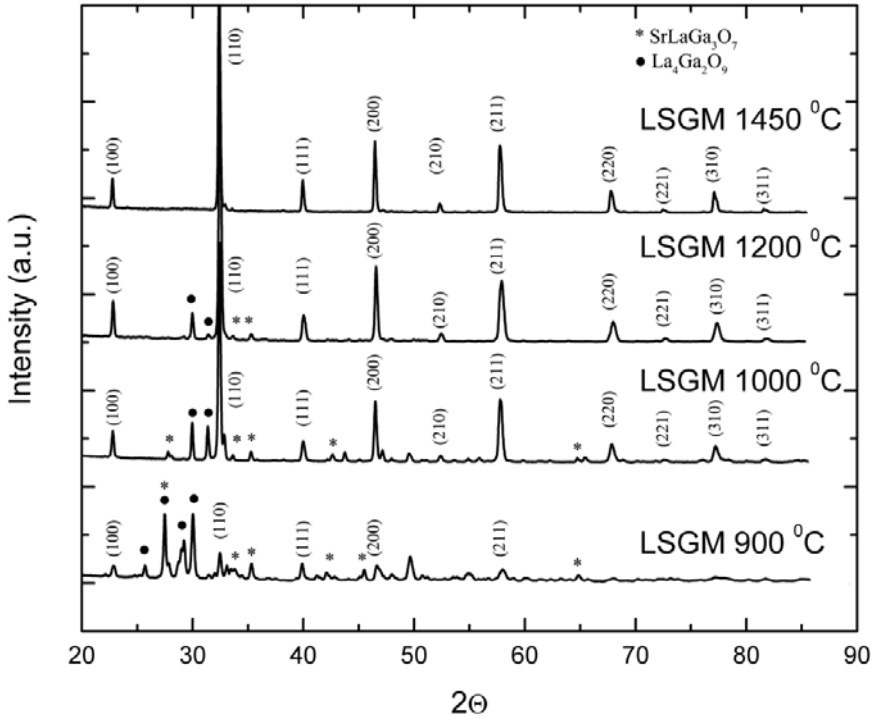

Fig 1. XRD patterns of the calcinated LSGM powders at 900 °C, 1000 °C and 1200 °C and sintered ceramic at 1450 °C for 6 h.

2. XPS results

Fig. 2 exhibits the superimposed XPS spectra of La 3d, Sr 3d, Ga 2p, Mg 1s for all calcined LSGM powders and the sintered sample at 1450 °C /6 h. The accuracy for Binding Energies (BEs) assignments was ± 0.2 eV.

The La 3 $d_{5/2}$ core level (BE = 834.02 eV) spectra is dominated by multi electron processes leading to a double peak spin–orbit component with separation between peaks of 3.9 eV [14]. This structure has been explained by an interatomic charge transfer from the ligand O 2p orbital to the empty La 4f* level occurring in parallel with the creation of the La 3d core hole (shake-up process) or by a strong final state mixing electronic configuration [14, 15].

Sr 3d band-like XPS spectrum shows multiple components. After a careful fitting procedure were identified four components, namely two 3 $d_{5/2}$– 3 $d_{3/2}$ doublets with 1.8 eV splitting between 3 $d_{5/2}$ and 3 $d_{3/2}$ peaks, a value in good agreement with previously published data [16, 17]. The 3 $d_{5/2}$ peaks were at 133.9 and 132.1 eV, respectively. The most intense 3 $d_{5/2}$ component (at 133.9 eV) is attributable to Sr^{2+} in the perovskite lattice, quite similar to those measured in similar perovskite structures [18, 19]. The BE of 3 $d_{5/2}$ component (at 132.1 eV) was close to that of $SrO_{1-\delta}$ suboxide (132.2 eV) [20]. and it can be ascribed to Sr^{2+} ions surrounded by vacancies in the oxygen-deficient perovskite structure [21].

The XPS spectra for gallium from all samples were similar to Ga_2O_3 standard suggesting the presence of Ga^{3+} state in all samples, with the BE value of the Ga $2p_{3/2}$ level at 1117.2 eV. The BE of the Mg KLL at 303.57 eV is close to that previously reported for Mg^{2+} in LSGM by Shkerim et al [19].

Fig. 3 shows the superimposed XPS spectra of the O 1s for all calcined LSGM powders. The O 1s core level spectra exhibit doublet feature with the peak energies at 530.4 eV and 533 eV for the sample calcinated to higher temperature the later suggesting the presence of non-bridging oxygens from $LaSrGa_3O_7$ which due to its melilite structure exhibits high interstitial oxide-ion conductivity [22, 23].

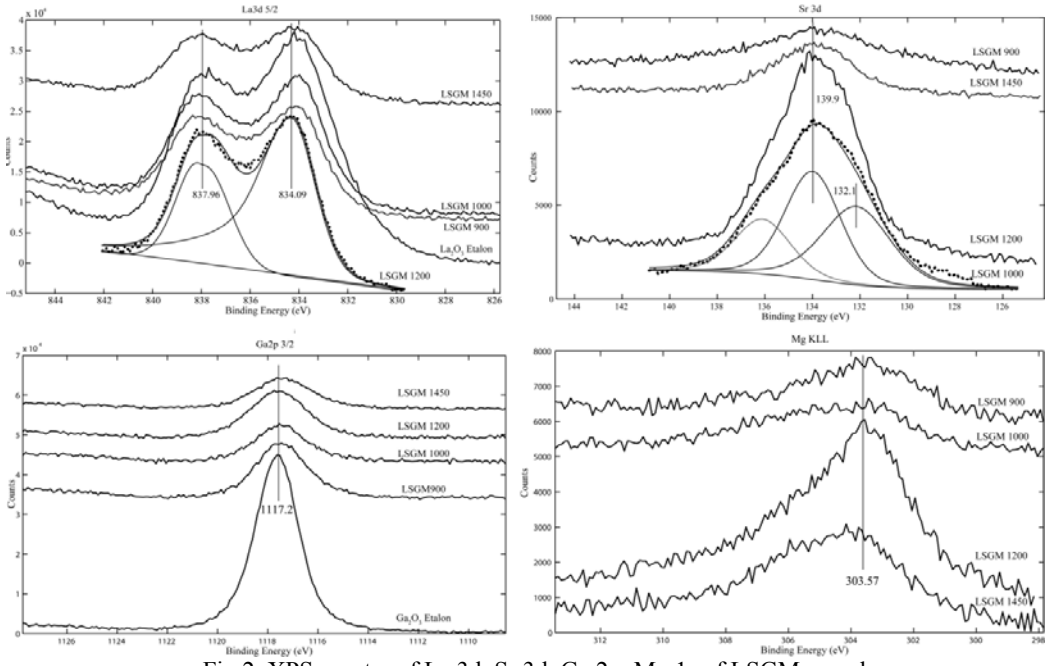

Fig 2. XPS spectra of La 3d, Sr 3d, Ga 2p, Mg 1s of LSGM samples

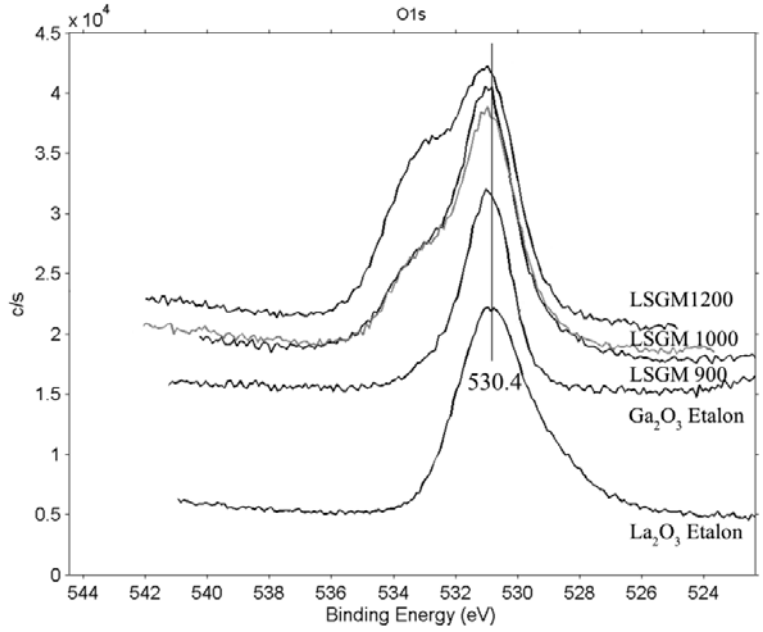

Fig 3. XPS spectra of O 1s of LSGM samples

3.3. Electrical proprieties

The conductivity in air of LSGM material is expected to be mostly ionic at high temperature with a transport number of oxygen ions larger than 0.8 at T ≥ 600 ºC, and its electric conductivity is almost independent of the oxygen partial pressure [24]. Therefore, the electrical characterization of LSGM materials were carry out in air at temperatures up to about 827 ºC.

The impedance spectra for sample LSGM 1000 measured at 227 ºC, 327 ºC and 377 ºC are presented in Fig. 4 a, b, and c. At lower temperatures (227 ºC, 327 ºC) the impedance spectra have three distinct regions: first distorted semicircle at high frequencies which correspond to the bulk conductivity, the second distorted semicircle which correspond to the grain boundary conductivity and the third region from lower frequencies which is attributed to the oxygen ion diffusion through the sample/contact electrode interface which is not of interest for further investigation. With the increasing of temperature the ionic conductivity increase and the semicircles are shifted to the frequencies higher than 1 MHz.

The transport of oxygen ion through the LSGM samples can be model using the equivalent electric circuit which has the same frequencies response as the sample. In case of LSGM ceramics a series of two parallel circuits of a resistance (Rgi – grain interior resistance, Rgb – grain boundary resistance) and a constant phase element (CPE) [25] have to be considered. The bulk and the grain boundary processes it is not possible to fit using a simple RC circuit because both processes exhibit a distribution of relaxation times (the semicircles are distorted). This behavior can be described by CPE which its impedance Z_{CPE} is given by:

$Z_{CPE} = \frac{1}{C(i\omega)^{1-\alpha}}$, where ω is the angular frequency and C and $\alpha \in [0,1]$ are frequency independent constants. The total resistance of the samples, R, was given by $R = Rb + Rgb$. The specific conductivities of the samples were calculated from impedance data using the formula:

$\sigma = \frac{t}{A \times R}$ where t and A represent the thickness and area of the sample surface.

Fig. 4 (d) shows Arrhenius plots of the total ionic conductivity for the LSGM samples. The sample LSGM 1200 exhibited larger electrical conductivities than the other samples maybe because, in these samples, the insulating secondary phases as $SrLaGa3O_7$ were still present. However, the value of conductivity of sample LSGM 1000 at 627 °C was 8.5 mS/cm which is larger than that of yttria-stabilized zirconia (YSZ, 8.1 mS/cm at 700 °C) [26]. The total conductivity of LSGM 1200, LSGM 1000 and LSGM 900 at 627 °C (at typical operating temperature for IT-SOFCs), were 15 mS/cm, 8.5 mS/cm and 3 mS/cm, respectively. Also, the electrical conductivities of all samples at 500 °C were

larger than the conductivities of LSGM obtained in our group by solid state method [27].

The apparent activation energy of electrical conductivity at for the total conductivity was determined by fitting the conductivity data to the Arrhenius relation[28]:

$$\sigma = A\exp(-\frac{Ea}{RT})$$

where Ea is the activation energy for migration of O^{2-} ions, R is the gas constant, T is absolute temperature, and A is the pre-exponential factor contains several constants. The apparent activation energies for conduction, calculated from the slopes of Arrhenius plots in the low and high temperature ranges are given in Table 1 and were in good agreement with previously published data [24, 29].

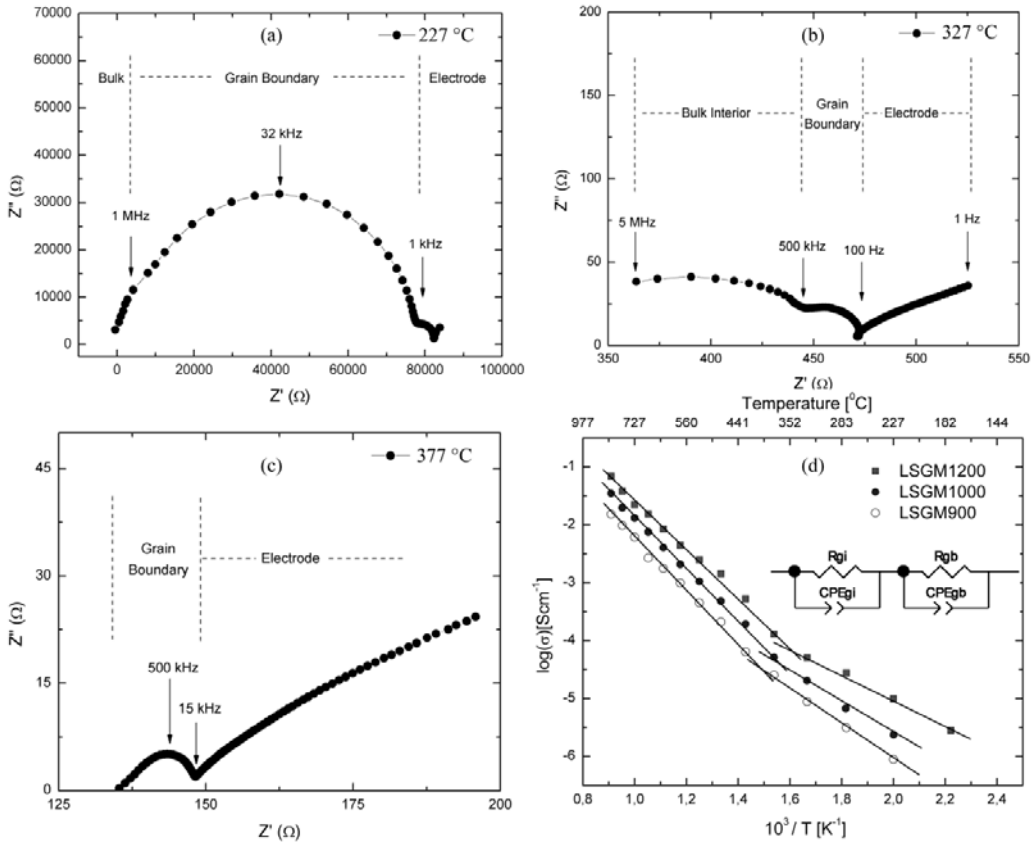

Fig 4. Impedance spectra of sintered sample LSGM 1000 measured at different temperatures (a, b, c). The frequency increases from right to left. The Arrhenius plot of total conductivities of the LSGM samples (d). The equivalent electrical circuit used to fit the impedance experimental data is shown in the inserted plot.

The Arrhenius plots have two linear regions, one with higher slopes (higher apparent activation energies) at high temperatures where the ionic conductivity is predominant [24] and other at lower temperatures with lower slopes (lower apparent activation energies) due to the electron hole conduction via a small polaron mechanism [29, 30].

Tabel 1

Total electrical conductivities (at 627 °C) and apparent activation energies (Ea) of the LSGM samples

Sample	Conductivity at 627 °C [mS/cm]	Ea (T<350 °C) [eV]	Ea (T>350 °C) [eV]
LSGM 900	3	0.26	0.43
LSGM 1000	8	0.24	0.42
LSGM 1200	15	0.18	0.41

4. Conclusions

The sol–gel method allowed preparing of dense and pure-phase LSGM sintered pellets with controlled composition. Sintering times as 6 h at 1450 °C were sufficient to obtain pellets with fractional density larger than 94% and with no presence of impurity phases as $SrLaGaO_4$.

XPS data confirmed the presence of all dopants in the material and two different chemical states for Sr^{2+} and oxygen, both related to the oxygen-deficient perovskite structure of LSGM.

Although the secondary phases in the samples calcinated below 1200 °C and sintered at 1450 °C for 6 h were not detectable by XRD, the electrical conductivities measured by impedance spectroscopy shown that the sample pre-calcinated at 1200 °C display a higher electrical conductivity. However, the value of conductivity of the sample LSGM 1000 at 627 °C was 8.5 mS/cm, which is larger than that of yttria-stabilized zirconia. The ionic conductivity dominated at temperatures of interest for IT-SOFCs, while hole conduction *via* polaron mechanism prevailed at lower temperatures. The physical chemical and electrical characterization demonstrated the ability of sol–gel methods to produce promising LSGM solid electrolytes for intermediate-temperature SOFCs.

Acknowledgements

The author Rareş Scurtu acknowledges the support of the Sectorial Operational Programme Human Resource Development (SOPHRD) under the contract number POSDRU/89/1.5/S/63700.

R E F E R E N C E S

[1] *Fergus, J.; Fergus, J.; Li, X.*, Solid Oxide Fuel Cells: Materials Properties and Performance, CRC: (2008).
[2] *Vielstich, W.; Yokokawa, H.; Gasteiger, H. A.*, Handbook of fuel cells: fundamentals, technology, and applications. Advances in electrocatalysis, materials, diagnostics and durability, part 5, Wiley: (2010).
[3] *Brett, D.; Atkinson, A.; Brandon, N.; Skinner, S.*, Chem. Soc. Rev., 2008, **37**, pp. 1568-1578.
[4] *Bozza, F.; Polini, R.; Traversa, E.*, Electrochem Commun, 2009, **11**, pp. 1680-1683.
[5] *Ishihara, T.; Matsuda, H.; Takita, Y.*, J. Am. Chem. Soc., 1994, **116**, pp. 3801-3803.
[6] *Huang, K.; Goodenough, J. B.*, J. Solid State Chem., 1998, **136**, pp. 274-283.
[7] *Huang, K.; Feng, M.; Goodenough, J.*, J. Am. Ceram. Soc., 1996, **79**, pp. 1100-1104.
[8] *Lybye, D.; Nielsen, K.*, Solid State Ionics, 2004, **167**, pp. 55-63.
[9] *Ishihara, T.*, Bull. Chem. Soc. Jpn., 2006, **79**, pp. 1155-1166.
[10] *Fergus, J. W.*, J of Power Sources, 2006, **162**, pp. 30-40.
[11] Pechini, M. P., US Patent, (1967).
[12] *Stevenson, J.; Armstrong, T.; McCready, D.; Pederson, L.; Weber, W.*, J. Electrochem. Soc., 1997, **144**, p 3613.
[13] Johnson, D., Zview, In Scribner Associates, Inc.: (2010).
[14] *Bolwin, K.; Schnurnberger, W.; Schiller, G.*, Zeitschrift für Physik B Condensed Matter, 1988, **72**, pp. 203-209.
[15] *Natile, M. M.; Ugel, E.; Maccato, C.; Glisenti, A.*, Appl. Catal., B, 2007, **72**, pp. 351-362.
[16] *Dupin, J. C.; Gonbeau, D.; Vinatier, P.; Levasseur, A.*, Phys. Chem. Chem. Phys., 2000, **2**, pp. 1319-1324.
[17] *Shin, J.; Kalinin, S.; Lee, H.; Christen, H.; Moore, R.; Plummer, E.; Baddorf, A.*, Surf. Sci., 2005, **581**, pp. 118-132.
[18] *Wang, P.; Yao, L.; Wang, M.; Wu, W.*, Journal of Alloys and Compounds, 2000, **311**, pp. 53-56.
[19] *Shkerin, S.; Bronin, D.; Kovyazina, S.; Gorelov, V.; Kuzmin, A.; Martemyanova, Z.; Beresnev, S.*, Solid State Ionics, 2004, **171**, pp. 129-134.
[20] *Machkova, M.; Brashkova, N.; Ivanov, P.; Carda, J. B.; Kozhukharov, V.*, Appl Surf Sci, 1997, **119**, pp. 127-136.
[21] *Polini, R.; Falsetti, A.; Traversa, E.; Schäf, O.; Knauth, P.*, J Eur Ceram Soc, 2007, **27**, pp. 4291-4296.
[22] *Kuang, Xiaojun*, *et al.,* Nature materials, 7, **6**, 2008, 498-504.
[23] *Malavasi, Lorenzo, Craig AJ Fisher, and M. Saiful Islam*, Chem. Soc. Rev., 39, **11**, 2010, 4370-4387.
[24] *Ishihara, T.; Furutani, H.; Honda, M.; Yamada, T.; Shibayama, T.; Akbay, T.; Sakai, N.; Yokokawa, H.; Takita, Y.*, Chem. Mater., 1999, **11**, pp. 2081-2088.
[25] *Macdonald, J.*, Solid State Ionics, 2005, **176**, pp. 1961-1969.
[26] *Cong, L.; He, T.; Ji, Y.; Guan, P.; Huang, Y.; Su, W.*, Journal of Alloys and Compounds, 2003, **348**, pp. 325-331.
[27] *Fruth, V.; Andronescu, C.; Hornoiu, C.; Enea, E.; Rusu, A.; Scurtu, R.*, Romanian Journal of Materials, 2011, **41**, pp. 56-63.
[28] *West, A. R.*, Solid State Chemistry and Its Applications, Wiley: (1991).
[29] *Stevenson, J.; Hasinska, K.; Canfield, N.; Armstrong, T.*, J. Electrochem. Soc., 2000, **147**, pp. 3213-3218.
[30] *Goodenough, J. B.*, Annu. Rev. Mater. Res., 2003, **33**, pp. 91-128.